Efficiency Optimization of Ge-V Quantum Emitters in Single-Crystal Diamond upon Ion Implantation and HPHT Annealing

Elena Nieto Hernández, Elisa Redolfi, Claudia Stella, Greta Andrini, Emilio Corte, Selene Sachero, Sviatoslav Ditalia Tchernij, Fabio Picariello, Tobias Herzig, Yuri M. Borzdov, Igor N. Kupriyanov, Alexander Kubanek, Paolo Olivero, Jan Meijer, Paolo Traina, Yuri N. Palyanov, and Jacopo Forneris*

The authors report on the characterization at the single-defect level of germanium-vacancy (GeV) centers in diamond produced upon Ge⁻ ion implantation and different subsequent annealing processes, with a specific focus on the effect of high-pressure-high-temperature (HPHT) processing on their quantum-optical properties. Different post-implantation annealing conditions are explored for the optimal activation of GeV centers, namely, 900 °C 2 h, 1000 °C 10 h, 1500 °C 1 h under high vacuum, and 2000 °C 15 min at 6 GPa pressure. A systematic analysis of the relevant emission properties, including the emission intensity in saturation regime and the excited state radiative lifetime, is performed on the basis of a set of ion-implanted samples, with the scope of identifying the most suitable conditions for the creation of GeV centers with optimal quantum-optical emission properties. The main performance parameter adopted here to describe the excitation efficiency of GeV centers as single-photon emitters is the ratio between the saturation optical excitation power and the emission intensity at saturation. The results show an up to eightfold emission efficiency increase in HPHT-treated samples with respect to conventional annealing in vacuum conditions, suggesting a suitable thermodynamic pathway toward the repeatable fabrication of ultra-bright GeV centers for single-photon generation purposes.

1. Introduction

Color centers in diamond represent an emerging class of solid-state systems for single-photon emission,[1–8] with appealing applications in quantum-enhanced technologies, including quantum information processing and quantum sensing.[9–18] Among them, point-defects related to group-IV impurities have displayed promising properties in terms of high photon emission rate, relatively narrow spectral signatures, and spin-dependent emission properties.[19–26]

The identification of reliable pathways toward their reproducible fabrication is therefore crucial for a widespread adoption of these systems. The most convenient method to date is represented by the fabrication by ion implantation and subsequent high-temperature annealing, which enables in perspective the control on both the position and the number of individual emitters on a diamond chip.[19,27–29] It is therefore

E. Nieto Hernández, E. Redolfi, C. Stella, E. Corte, S. Ditalia Tchernij, P. Olivero, J. Forneris
Department of Physics
University of Torino
Torino 10125, Italy
E-mail: jacopo.forneris@unito.it
E. Nieto Hernández, E. Redolfi, G. Andrini, E. Corte, S. Ditalia Tchernij, P. Olivero, J. Forneris
Istituto Nazionale di Fisica Nucleare (INFN)
sezione di Torino
Torino 10125, Italy

The ORCID identification number(s) for the author(s) of this article can be found under https://doi.org/10.1002/qute.202300010

C. Stella, S. Ditalia Tchernij, F. Picariello, P. Olivero, P. Traina, J. Forneris
Istituto Nazionale di Ricerca Metrologica (INRiM)
Torino 10135, Italy
G. Andrini
Department of Electronics and Communications
Politecnico di Torino
Torino 10129, Italy
S. Sachero, A. Kubanek
Institute for Quantum Optics
Universität Ulm
D-89069 Ulm, Germany
T. Herzig, J. Meijer
Applied Quantum Systems, Felix-Bloch Institute for Solid-State Physics
Universität Leipzig
04103 Leipzig, Germany
Y. M. Borzdov, I. N. Kupriyanov, Y. N. Palyanov
V.S. Sobolev Institute of Geology and Mineralogy
Siberian Branch of the Russian Academy of Sciences
Academician Koptyug Ave., 3, Novosibirsk 630090, Russian Federation

**ADVANCED
SCIENCE NEWS**

www.advancedsciencenews.com

**ADVANCED
QUANTUM
TECHNOLOGIES**

www.advquantumtech.com

crucial to define optimal post-implantation processing schemes, thus ensuring both the efficient formation of optically active color centers upon the implantation of individual ions[29–31] and guaranteeing optimal photon emission properties.[32,33]

One of the most significant limitations toward the reliable fabrication of group-IV-related emitters lies in the sub-optimal incorporation of atomically large impurities in the highly dense host diamond crystal upon irradiation at keV energies, which results in substantial lattice distortions[34,35] and residual radiation damage[36,37] affecting their emission properties, despite the adoption of annealing post-implantation processes up to 1200 °C temperature. A possible solution has been hinted for SnV and PbV centers by the adoption of high-pressure high-temperature (HPHT) post-implantation annealing. In these systems, treatments at 2100 °C temperature and 7.7 GPa pressure in keV-ion-implanted diamond which resulted in improved spectral emission properties and reduced contributions from competing impurity-related defect configurations.[3,38] Nevertheless, a systematic comparison of the effects on the single-photon emission properties of HPHT treatment with respect to conventional annealing processes has not been performed to date in the scientific literature. This work addresses this investigation on the group-IV-related germanium-divacancy complex (GeV center).[5,29,35] An emphasis is given toward the physical parameters needed to maximize the emission efficiency, in terms of optical excitation power and emission intensity, in order to optimize the throughput of generated photons with a minimal excitation energy.

2. Experimental and Results

2.1. Samples Preparation

The experiments were performed on three single-crystal type-IIa diamond samples supplied by ElementSix. Samples #1 and #2 were consisted of $2 \times 2 \times 0.5$ mm^3 "electronic grade" quality substrates, characterized by <5 ppb substitutional N and B concentrations. Sample #3 was consisted of a $3 \times 3 \times 0.3$ mm^3 "optical grade" substrate with nominal substitutional concentrations of $N_S < 1$ ppm and $B_S < 0.05$ ppm. Samples were implanted with 40 keV Ge$^-$-ions at the low energy accelerator of the University of Leipzig. Several regions of $\approx 200 \times 200$ µm^2 area were implanted at fluences in the 10^{10}–10^{13} cm^{-2} range by means of a collimating mask. Generally, the fluence values were too high to enable a direct investigation of GeV centers at the single-emitter level within the implantation regions. Therefore, the analysis was carried in correspondence of the outer edges of the implanted regions, where individual color centers were formed due to the implantation of stray ions upon scattering with the collimating mask. No noticeable statistical differences were observed in the emission parameters of single GeV centers at the outer edges of regions implanted at different fluences. Sample #1 underwent two subsequent post-implantation annealing processes in vacuum (i.e., at pressures $<5 \times 10^{-6}$ mbar), namely, 900 °C (2 h duration), 1000 °C (10 h duration). Sample #2 was processed at 1500 °C for 1 h in vacuum. Sample #3 underwent an annealing treatment at 950 °C (after which no individual GeV centers could

be isolated due to the intense background emission of native NV centers), followed by a 15 min annealing performed at 2000 °C under 6 GPa pressure for 15 min (referred to as "HPHT annealing" in the following).

2.2. Effects of HPHT Annealing

The HPHT treatment was performed at the IGM SB RAS (Novosibirsk) under a stabilizing pressure of about 6 GPa via a split-sphere multi-anvil apparatus (BARS).[39] Cesium chloride (CsCl) was used as pressure transmitting medium, providing quasi-hydrostatic conditions of annealing. The sample was annealed at ≈ 2000 °C for 15 min. As an increase of surface roughness was expected on the basis shown of previous studies on HPHT annealing of different classes of emitters,[40] a morphological assessment of the sample surface was performed by means of scanning electron microscope (SEM) imaging. The SEM map acquired from Sample #1 following 950 °C thermal annealing is shown in **Figure 1**a, to be compared with the morphology of Sample #3 surface upon HPHT annealing (Figure 1b). Sample #3 exhibits an inhomogenous increase in the surface roughness of the sample, denoted by both the growth of µm-sized seeds due to the HPHT conversion to diamond, to a much lesser extent, high-temperature-induced surface etching, indicating that the processing parameters for the HPHT annealing still require some optimization. Nevertheless, the confocal photoluminescence (PL) maps acquired from Sample #3 (Figure 1c) in the outer region of a Ge-implanted area are comparable with those obtained from Sample #1 (Figure 1d) and Sample #2. It can thus be concluded that increased surface roughness induced by the HPHT treatment did not hinder the formation of stable single-photon emitters.

The HPHT process outcome was monitored by comparing PL ensemble spectra acquired at liquid nitrogen temperature from the region implanted at 3×10^{12} cm^{-2} fluence before and after the treatment using a custom-built setup based on a Horiba JY iHR320 monochromator equipped with a Syncerity CCD detector. **Figure 2** shows the PL spectra acquired under 395 nm (Figure 2a) and 532 nm (Figure 2b) excitations, both before and after processing. Prior to the HPHT process, the spectra (black lines) are dominated by native NV centers emission with zero-phonon lines (ZPLs) at 575 and 637 nm,[41] whose intensity is significantly higher than that of the GeV centers (ZPL at 602 nm[5,13]). In addition, an emission band characterized by a ZPL at 467.7 nm (2.65 eV) and phonon replicas with 73 meV energy was observed in the spectrum excited with 395 nm, which is tentatively attributed to intrinsic vacancy-related defects.[42] Following the HPHT treatment, the PL spectra recorded from the same region (red line in Figure 2a,b) showed the complete disappearance of both the 467.7 nm feature and the NV-center-related emissions. This result is line with previous reports indicating the disaggregation of the NV and 467.7 nm centers at temperatures 1500–1700[43,44] and ≈ 1900 °C,[42] respectively. Consequently, the GeV center appears as the dominant PL feature after HPHT annealing. Furthermore, its relative intensity with respect to the first-order diamond Raman line appears significantly increased.
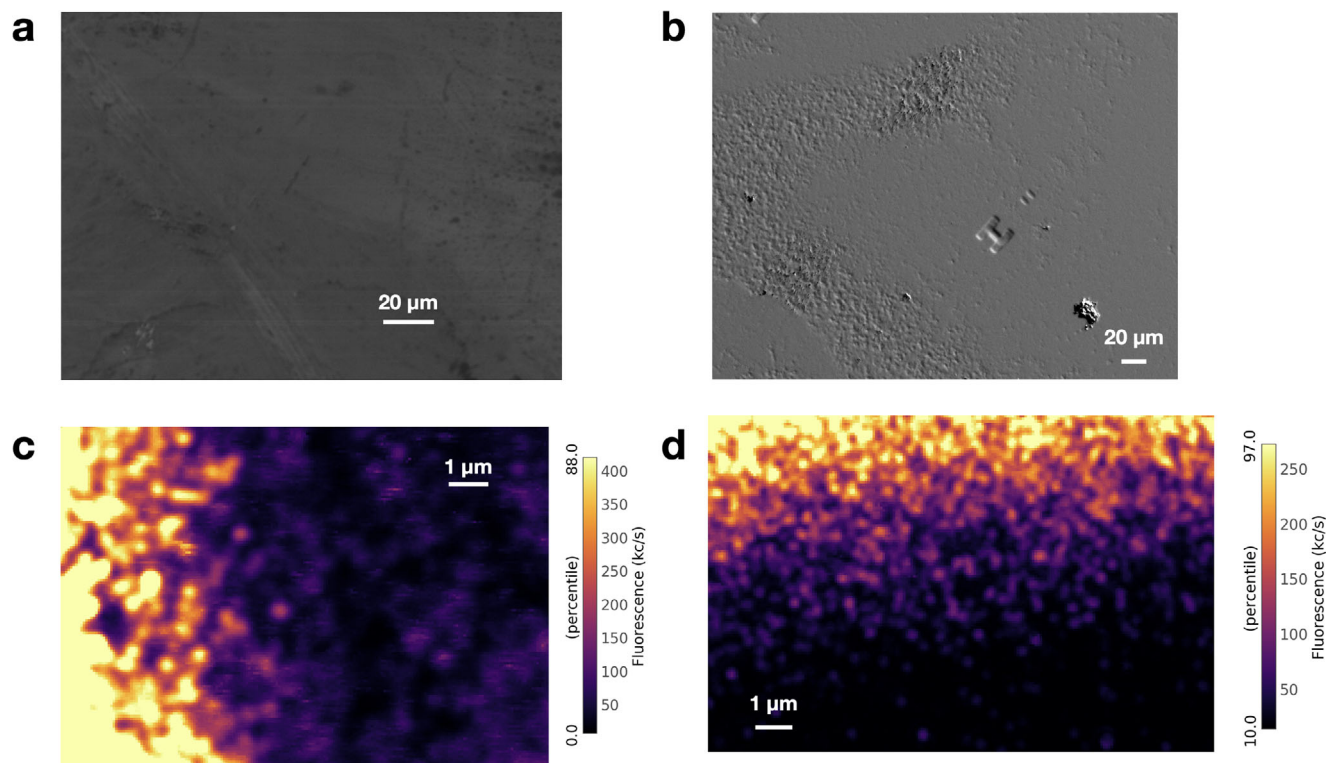
**ADVANCED
SCIENCE NEWS**

www.advancedsciencenews.com

**ADVANCED
QUANTUM
TECHNOLOGIES**

www.advquantumtech.com

Figure 1. SEM image of the a) Sample #1 following 950 °C annealing in vacuum and b) Sample #3 after the HPHT treatment. The reference "H" marker at the center of the image was fabricated by focused-ion-beam milling prior to HPHT annealing. PL confocal microscopy map of the outer edge of a region implanted with 40 keV Ge⁻ ions on c) Sample #3 and d) Sample #1.
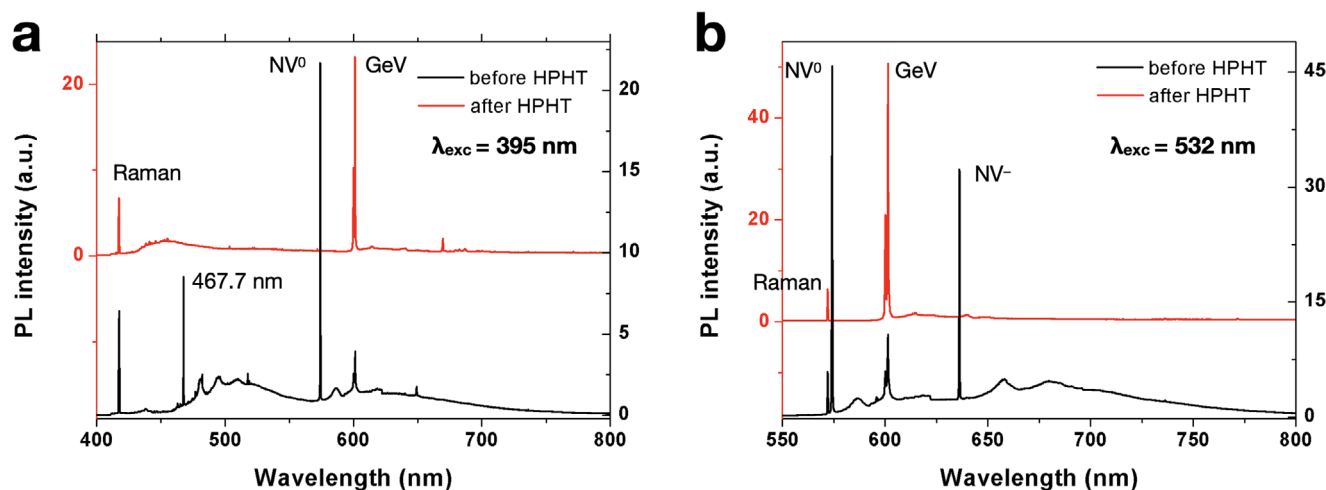

Figure 2. PL spectra acquired from Sample #3 under a) 395 and b) 532 nm CW laser excitation before (black line) and after (red line) HPHT annealing.

2.3. Single-Photon PL Emission Characterization

Each of the above-described treatments was followed by a systematic characterization at the single-photon emitter level in PL regime. The analysis was performed using a custom fiber-coupled single-photon-sensitive custom confocal microscope (100× air objective, 0.9 NA) under 520 nm CW laser excitation. A dichroic mirror and a set of optical filters ensured the detection of

>550 nm wavelengths. The PL spectra were acquired with a single grating monochromator (1200 grooves mm⁻¹, 600 nm blaze, ≈4 nm spectral resolution) out-coupled via multimode fibers to a single photon avalanche diode (SPAD). The confocal microscope was equipped with a Hanbury-Brown and Twiss (HBT) interferometer, allowing the experimental characterization of single-photon emitters via the analysis of the second-order autocorrelation function.[1] The HBT interferometer was implemented by
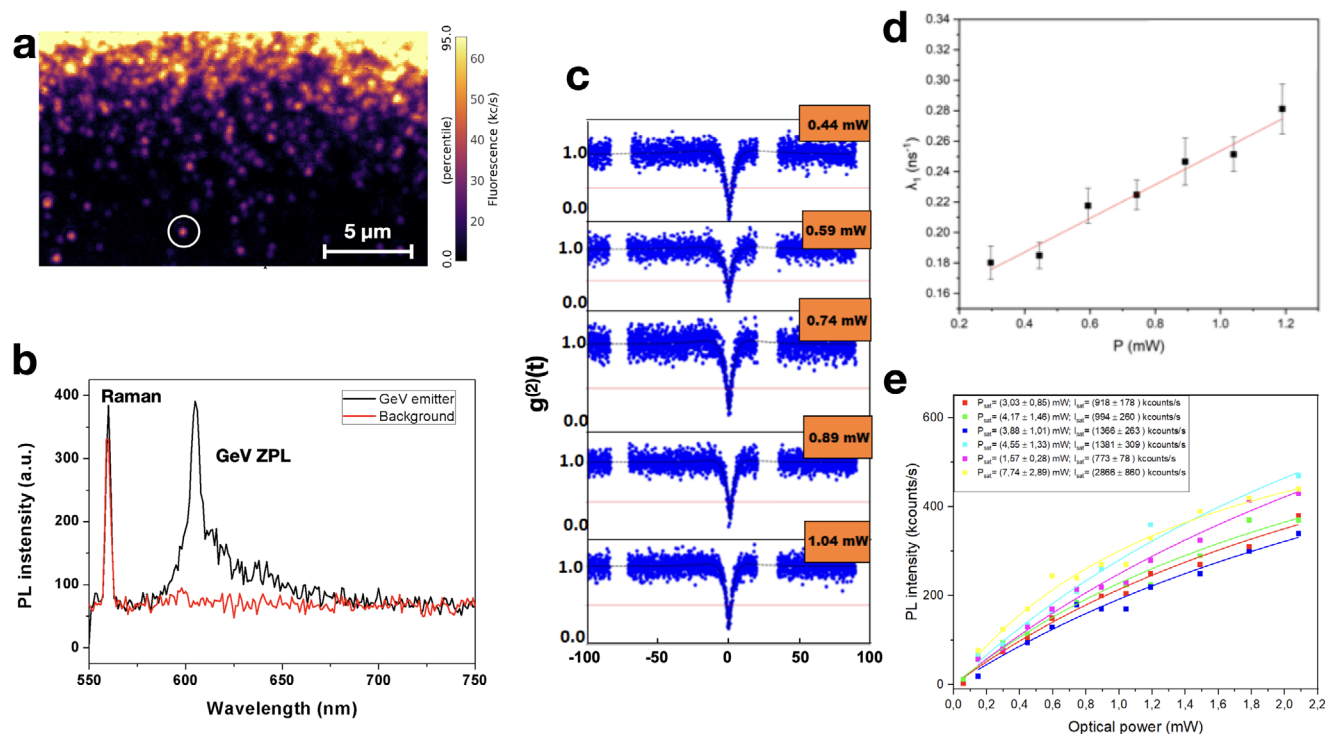
Figure 3. Exemplary steps in the systematic analysis of individual GeV centers formed by ion implantation and annealing. a) PL map of the outer edge of a region implanted with 40 keV Ge-ions and annealed at 900 °C for 2 h in vacuum. b) PL spectrum acquired under 520 nm CW laser excitation from the diffraction-limited spot (black line) circled in white in Figure 2a and from a pristine region of the sample (red line). c) Second-order autocorrelation chronograms acquired from the same spot under 0.44, 0.59, 0.74, 0.89, and 1.04 mW excitation powers. The dashed black lines indicate the fitting curves based on a three-level model. c) Linear regression of the λ_1 fitting parameter as a function of the optical excitation power. d) Intensity saturation curves of six individual GeV centers acquired from Sample #1.

a fiber-fused 50:50 beamsplitter connected to two independent SPADs.[45]

An assessment of the dependence of the emission properties of the GeV centers from the post-implantation treatment was then performed by means of a systematic study at the single-photon emitter level. The study was based on the following sampling: 15 GeV centers in Sample #1 following both the 900 and 1000 °C annealing in vacuum; 13 GeV centers in Sample #2 following the 1500 °C treatment in vacuum; 15 centers in Sample #3 following the HPHT process. The adopted experimental approach was the following for all the considered annealing conditions. First, PL mapping was performed to identify bright emission spots as potential single-photon emitters. **Figure 3a** shows an exemplary PL map acquired from the outer edge of a region of Sample #1 implanted at 3×10^{12} cm^{-2} fluence and subsequently annealed at 900 °C for 2 h in vacuum conditions. The color scale encodes the PL intensity value, in kcounts per second (kcps). The upper part of the map, corresponding to higher PL counts, is closer (i.e., few μm) to the edge of the implanted region and is thus denoted by a higher concentration of GeV centers. The spatial gradient toward lower PL intensity at increasing distance from the implanted region enables the identification of individual diffraction-limited spots, each of which potentially corresponds to an individual to single GeV emitters. Each emitting spot was characterized by PL spectroscopy to verify the occurrence of the GeV spectral fingerprint at 602 nm. Figure 3b shows as an example the typical emission spectrum (black line)

observed from the spot highlighted by a white circle in Figure 3a at an excitation power of 0.6 mW, to be compared with the background spectrum acquired from a pristine region of the same sample (red line). The verification of the occurrence of individual GeV emitters was then validated by analyzing the background-subtracted HBT interferograms acquired under different excitation powers (Figure 3c).

The second-order autocorrelation chronograms were fitted according to the three-level system expression[46]

$$g^{(2)}(t) = 1 - A_1 \cdot \exp\left(-\lambda_1|t|\right) + A_2 \cdot \exp\left(-\lambda_2|t|\right) \quad (1)$$

where the A_1 parameter provides an estimate of the antibunching effect at $t = 0$ delay, and the λ_1 parameter (i.e., the reciprocal of the characteristic time constant) depends on the optical excitation power P through a linear coefficient α

$$\lambda_1 = \lambda_1(P) = \alpha \cdot P + \tau^{-1} \quad (2)$$

The study of the power-dependence of the A_2 and λ_2 parameters related to the system's shelving state was beyond the scope of this work, due to the overall weak bunching effect observed in all the considered emitters. The observation of a $g^{(2)}(t = 0)$ value well below (i.e., an A_1 parameter well above) 0.5 was adopted as the criterion to assess a single-photon emission from the considered diffraction-limited spot. The acquired second-order autocorrelation chronograms were also adopted to gain information on
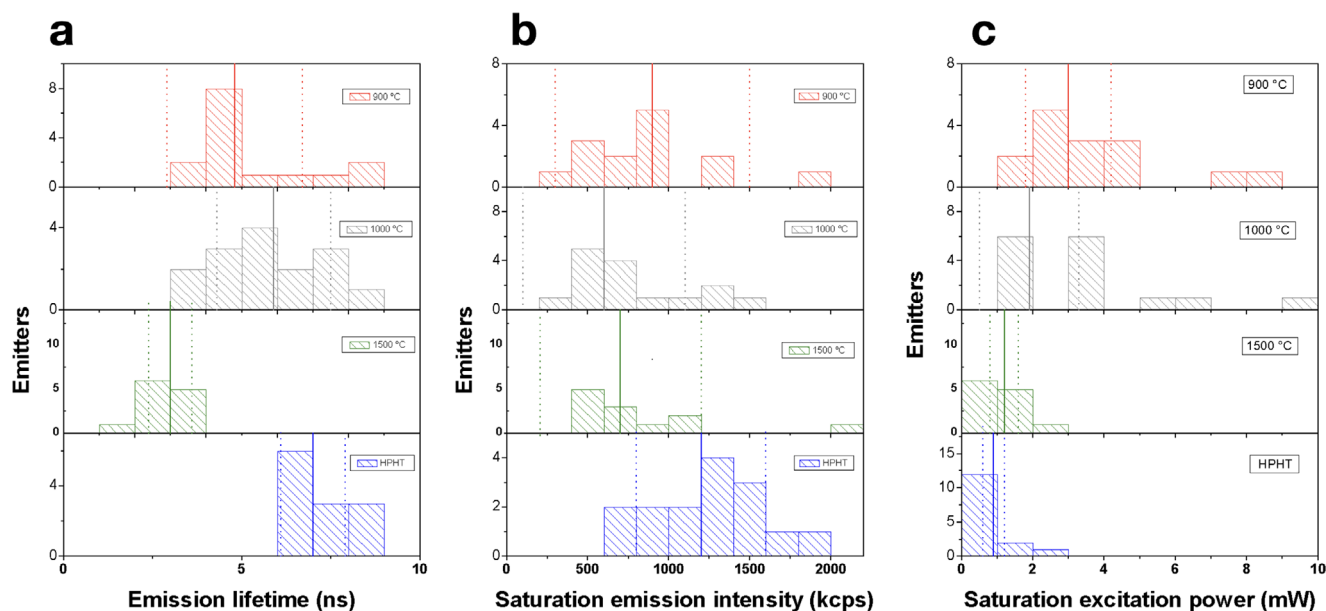
**ADVANCED
SCIENCE NEWS**
www.advancedsciencenews.com

**ADVANCED
QUANTUM
TECHNOLOGIES**
www.advquantumtech.com

Figure 4. Histograms of the occurrence of a) emission lifetime, b) saturation emission intensity, and c) saturation excitation power, among a set of 57 single-photon emitters grouped by post-implantation annealing treatment. The color codes the different annealing temperatures (red: 900 °C, gray: 1000 °C, green: 1500 °C, blue: HPHT treatment). The vertical continuous lines indicate the median value of each distribution. The dashed lines indicate the standard deviation as evaluated by the Q3−Q1 interquartile assuming a normal distribution.

Table 1. Table of the median values of excited state lifetime, emission intensity at saturation, and optical excitation power at saturation extracted from the analysis of the histograms in Figure 4.

Post-implantation treatment	Crystal quality	Median excited state radiative lifetime [ns]	Emission intensity at saturation [kcps]	Optical excitation power at saturation [mW]
900 °C 2 h	Electronic grade	4.8 ± 1.9	900 ± 600	3.0 ± 1.2
1000 °C 10 h	Electronic grade	5.9 ± 1.6	600 ± 500	3.1 ± 1.4
1500 °C 1 h	Electronic grade	3.0 ± 0.6	650 ± 350	1.2 ± 0.5
HPHT (2000 °C, 6 GPa)	Optical grade	7.0 ± 0.9	1200 ± 400	0.9 ± 0.3

the lifetime τ of the excited state of each GeV center through a linear regression of the (λ vs P) curve (Figure 3d) according to the relation $\tau = \lambda_1(P = 0)^{-1}$. As an example, Figure 3d shows the linear regression corresponding to the dataset reported in Figure 3c. Finally, the intensity saturation emission of individual GeV centers was determined by measuring the PL count rate I as a function of the excitation optical power, upon subtraction of the background count rate acquired from an unimplanted region. Figure 3d shows exemplary families of intensity saturation curves acquired from a set of individual GeV centers on Sample #1 following 900 °C annealing. All curves acquired from individual emitters were fitted according to the saturation model[2,29]

$$I(P) = I_{sat} \cdot P / (P + P_{sat}) \tag{3}$$

where I_{sat} and P_{sat} are the emission intensity and optical power at saturation, respectively. The above-described characterization method was applied to investigate the statistical distribution of the key parameters for single-photon emission (**Figure 4**): excited state radiative lifetime (Figure 4a), emission intensity at saturation (Figure 4b), and saturation excitation optical power (Figure 4c). The figures show the histograms of each parameter

for the four considered annealing processes. The median value of the distribution is superimposed to each histogram (continuous vertical line) together with the standard deviation (dashed lines), as derived from the Q3−Q1 interquartile difference, by assuming a normal distribution. These values are also reported in **Table 1**.

The statistical distribution of the emitters lifetime values (Figure 4a) did not highlight an apparent trend as a function of the considered annealing process. The median values for the 900 and 100 °C processes (i.e., 4.8 ± 1.9 and 5.9 ± 1.6 ns, respectively) are compatible with the results achieved both from the samples treated with the 1500 °C temperature (3.0 ± 0.6 ns) and HPHT (7.0 ± 0.9 ns) processes. Conversely, the latter two are not mutually compatible. The lifetime median values measured for the HPHT-treated crystal are compatible with those observed at the lowest annealing temperatures. This observation suggests that the adoption of an "optical grade" sample does not provide an environment-dependent modification (e.g., unintentional doping due to higher N contents of Sample #3) of the GeV emission properties with respect to "electronic grade" diamond. As a consequence, the HPHT treatment enables the utilization of cheaper material substrates for GeV-based technological applications. While such consideration is further supported (see below)

**ADVANCED
SCIENCE NEWS**

www.advancedsciencenews.com

**ADVANCED
QUANTUM
TECHNOLOGIES**

www.advquantumtech.com

by the enhancement in the emission efficiency of the GeV defect upon HPHT annealing, the technological perspective of this method will depend on the assessment of spectral diffusion associated with the residual density of the optically inactive impurities and defects typically present in a lower grade crystal.

To the best of our knowledge, a systematic assessment of the GeV emission lifetime based on a statistical analysis of emitters has not been performed prior to this work. Indeed, the lifetime values reported in literature cover a 1.4–6.6 ns range on the basis of previous reports on a limited numbers of probed individual GeV centers.[24,29]

Concerning the emission intensity at saturation, the median I_{sat} values obtained for the four different annealing conditions (respectively: 900 ± 600, 600 ± 500, 650 ± 350, and 1200 ± 400 kcps) are fully compatible. This is however the net result of the fact that the 900 and 1000 °C processes lead to a wide variability in the I_{sat} parameter. It is worth noting that the >600 kcps values reported for each of these datasets represent an appealing experimental evidence of the very promising quantum-optical performance of this system, particularly if compared with the results of previous room-temperature characterization (i.e., in the 178 ± 4 to 790 ± 20 kcps range[24,29]). Incidentally, several individual emitters exceeding 1 Mcps emission rates were identified in previous works, which could be partially explained assuming different detection efficiencies for the adopted experimental setup. While the overall data variability did not enable to identify any significant trend as a function of the annealing temperature, it is worth mentioning that 60% of the emitters studied in the HPHT-treated sample exhibited >1 Mcps intensity at saturation, suggesting a substantial positive effect of the process on the opto-physical properties of the GeV center.

The statistical distribution of the observed optical excitation powers at saturation is summarized in Figure 4c. Similarly to lifetime and emission intensity parameters, the data do not provide strong evidence of significant differences in the P_{sat} parameter for the 900 °C (3.0 ± 1.2 mW) and 1000 °C (3.1 ± 1.4 mW) annealing processes. These results are also consistent with previous reports on individual emitters, with excitation powers at saturation in the 4.5–4.7 mW range for annealing at 1000–1200 °C temperatures.[24,29] Remarkably, the saturation power is considerably reduced when the annealing temperature increases to 1500 °C (1.2 ± 0.5 mW), and it is further decreased to 0.9 ± 0.3 mW upon HPHT treatment. This observation is in line with a recently proposed model for group-IV impurities in diamond[47] relating the charge state stability with the concentration of surrounding lattice divacancies. Divacancy are introduced in the diamond lattice as a byproduct of the ion implantation process performed to fabricate GeV centers. Although divacancies are still present in HPHT-treated diamonds, the high-pressure annealing is reported to efficiently promote the disaggregation of such defects even for short processes.[48] If the divacancy is identified as the optically inactive defect interfering with the charge stability of the GeV center, then its disaggregation upon HPHT annealing could be regarded as the origin of the improved emission efficiency of the latter.

The overall performance of GeV centers as single-photon emitters can be parametrized by considering the ratio between the saturation optical excitation power and the emission intensity at saturation, $E_{sat} = P_{sat}/I_{sat}$. This parameter, which is inversely pro-

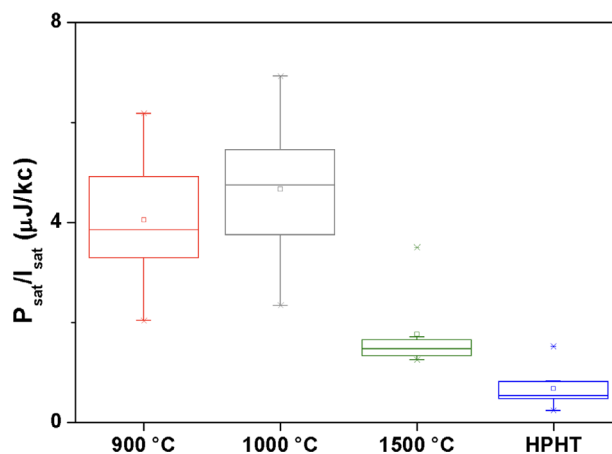**Figure 5.** Box chart of the P_{sat}/I_{sat} ratio extracted for different post-implantation annealing processes.

portional to the system quantum efficiency, can be regarded as an indicator of the effectiveness in the optical excitation and radiative response of the system. Lower values of E_{sat} indicate lower energy requested for single-photon emission, and thus a higher efficiency in the excitation–emission process. The achievement of low E_{sat} values is therefore a key requisite to enhance emission intensity with minimal optical power consumption, thus enabling ultra-bright emission from individual GeV centers. The same goal also offers to simultaneously address arrays of individual emitters (e.g., embedded in integrated photonic structures[49]) by using a single excitation source with modest optical output, thus minimizing heat dissipation and reducing the constraints on the device design. **Figure 5** shows box chart plots summarizing the distributions of the parameter evaluated for the populations of emitters under investigation. The decreasing trend of E_{sat} at increasing annealing temperatures is apparent, as the 1500 °C (1.5 ± 0.3 μJ kcps^{-1}) and the HPHT (0.5 ± 0.3 μJ kcps^{-1}) treatments lead to ×2.6 and ×7.8 increase with respect to the 900 °C annealing process (3.9 ± 1.6 μJ kcps^{-1}), respectively.

3. Conclusions

We reported on a systematic investigation of the main emission parameters (namely, excited state radiative lifetime, saturation excitation power, and emission intensity at saturation) of GeV centers fabricated in diamond upon implantation following different annealing conditions. Our results show a significant trend toward lower optical excitation powers at increasing annealing temperatures. This result likely corresponds to an increase in the emission intensity, although the rather large variability in the data did not enable the identification of an unambiguous trend in such parameter. The overall effectiveness of the excitation and emission processes is described by the ratio between emission intensity and optical excitation power at saturation, which exhibits an eightfold improvement for the HPHT-treated sample with respect to conventional thermal annealing at 900–1000 °C in vacuum conditions. This remarkable increase in the single-photon source efficiency can be potentially extended to other classes of quantum emitters in diamond[3,4,45] and in other host material platforms.[50,51] It suggests an effective and highly controllable

processing route on the road toward the creation of ultra-bright GeV centers with optimal emission properties for single-photon generation purposes and quantum technology applications. The results obtained are significant both at the individual emitter level and for the parallel excitation of multiple sources in integrated devices for quantum information processing[45,52,53] and metrology.[54,55]

Conflict of Interest

The authors declare no conflict of interest.

Data Availability Statement

The data that support the findings of this study are available from the corresponding author upon reasonable request.

[1] R. Brouri, A. Beveratos, J. Poizat, P. Grangier, *Opt. Lett.* **2000**, *25*, 1294.

[2] C. Wang, C. Kurtsiefer, H. Weinfurter, B. Burchard, *J. Phys. B* **2006**, *39*, 37.

[3] T. Iwasaki, Y. Miyamoto, T. Taniguchi, P. Siyushev, M H. Metsch, F. Jelezko, M. Hatano, *Phys. Rev. Lett.* **2017**, *119*, 253601.

[4] S. Ditalia Tchernij, T. Lühmann, T. Herzig, J. Küpper, A. Damin, S. Santonocito, M. Signorile, P. Traina, E. Moreva, F. Celegato, S. Pezzagna, I. P. Degiovanni, P. Olivero, M. Jakšić, J. Meijer, P. M. Genovese, J. Forneris, *ACS Photonics* **2018**, *5*, 4864.

[5] Y. N. Palyanov, I. N. Kupriyanov, Y. M. Borzdov, N. V. Surovtsev, *Sci. Rep.* **2015**, *5*, 14789.

[6] R. Sandstrom, L. Ke, A. Martin, Z. Wang, M. Kianinia, B. Green, W. B Gao, I. Aharonovich, *Opt. Commun.* **2018**, *411*, 182.

[7] G. Prestopino, M. Marinelli, E. Milani, C. Verona, G. Verona-Rinati, P. Traina, E. Moreva, I. P. Degiovanni, M. Genovese, S. Ditalia Tchernij, F. Picollo, P. Olivero, J. Forneris, *Appl. Phys. Lett.* **2017**, 111105, *111*.

[8] T. Lühmann, S. Diziain, J. Meijer, S. Pezzagna, *ACS Photonics* **2022**, *9*, 1691.

[9] C. H. Su, A. D. Greentree, L. C. L. Hollenberg, *Phys. Rev. A* **2009**, *80*, 052308.

[10] D. Chen, Z. Mu, Yu Zhou, J E. Fröch, A. Rasmit, C. Diederichs, N. Zheludev, I. Aharonovich, W-Bo Gao, *Phys. Rev. Lett.* **2019**, *123*, 33602.

[11] A. Sipahigil, M. L. Goldman, E. Togan, Y. Chu, M. Markham, D. J. Twitchen, A. S. Zibrov, A. Kubanek, M. D. Lukin, *Phys. Rev. Lett.* **2012**, *108*, 143601.

[12] S. Rodt, S. Reitzenstein, *APL Photonics* **2021**, *6*, 010901.

[13] J. W. Fan, I. Cojocaru, J. Becker, I. V. Fedotov, M. H. A. Alkahtani, A. Alajlan, S. Blakley, M. Rezaee, A. Lyamkina, Y. N. Palyanov, Y. M. Borzdov, Y. P Yang, A. Zheltikov, P. Hemmer, A V. Akimov, *ACS Photonics* **2018**, *5*, 765.

[14] J. Li, H. Ebendorff-Heidepriem, B C. Gibson, A D. Greentree, M R. Hutchinson, P. Jia, R. Kostecki, G. Liu, A. Orth, M. Ploschner, E P. Schartner, S C. Warren-Smith, K. Zhang, G. Tsiminis, E M. Goldys, *APL Photonics* **2018**, *3*, 100902.

[15] J. Jeske, D. W. M. Lau, X. Vidal, L. P. Mcguinness, P. Reineck, B. C. Johnson, M. W. Doherty, J. C. Mccallum, S. Onoda, F. Jelezko, T. Ohshima, T. Volz, J. H. Cole, B. C. Gibson, A. D. Greentree, *Nat. Commun.* **2017**, *8*, 14000.

[16] J. Forneris, S. Ditalia Tchernij, P. Traina, E. Moreva, N. Skukan, M. Jakšić, V. Grilj, F. Bosia, E. Enrico, G. Amato, I. P. Degiovanni, B. Naydenov, F. Jelezko, M. Genovese, P. Olivero, *Phys. Rev. Appl.* **2018**, *10*, 014024.

[17] R. Sakurai, Y. Kainuma, T. An, H. Shigekawa, M. Hase, *APL Photonics* **2022**, *7*, 066105.

[18] J. L. Webb, L. Troise, N. W. Hansen, L. F. Frellsen, C. Osterkamp, F. Jelezko, S. Jankuhn, J. Meijer, K. Berg-Sørensen, J. F. Perrier, A. Huck, U. L. Andersen, *Phys. Rev. Appl.* **2022**, *17*, 064051.

[19] C. Bradac, W. Gao, J. Forneris, M. E. Trusheim, I. Aharonovich, *Nat. Commun.* **2019**, *10*, 5625.

[20] M. E. Trusheim, B. Pingault, N. H. Wan, M. Gündoğan, L. De Santis, R. Debroux, D. Gangloff, C. Purser, K. C. Chen, M. Walsh, J. J. Rose, J. N. Becker, B. Lienhard, E. Bersin, I. Paradeisanos, G. Wang, D. Lyzwa, A. R. P. Montblanch, G. Malladi, H. Bakhru, A. C. Ferrari, I. A. Walmsley, M. Atatüre, D. Englund, *Phys. Rev. Lett.* **2020**, *124*, 023602.

[21] M. H. Metsch, K. Senkalla, B. Tratzmiller, J. Scheuer, M. Kern, J. Achard, A. Tallaire, M. B. Plenio, P. Siyushev, F. Jelezko, *Phys. Rev. Lett.* **2019**, *122*, 190503.

[22] P. Siyushev, M. H. Metsch, A. Ijaz, J. M. Binder, M. K. Bhaskar, D. D. Sukachev, A. Sipahigil, R. E. Evans, C. T. Nguyen, M. D. Lukin, P. R. Hemmer, Y. N. Palyanov, I. N. Kupriyanov, Y M. Borzdov, L J. Rogers, F. Jelezko, *Phys. Rev. B* **2017**, *96*, 081201.

[23] D. D. Sukachev, A. Sipahigil, C. T. Nguyen, M. K. Bhaskar, R. E. Evans, F. Jelezko, M. D. Lukin, *Phys. Rev. Lett.* **2017**, *119*, 223602.

[24] M. K. Bhaskar, D. D. Sukachev, A. Sipahigil, R. E. Evans, M. J. Burek, C. T. Nguyen, L. J. Rogers, P. Siyushev, M. H. Metsch, H. Park, F. Jelezko, M. Lončar, M. D. Lukin, *Phys. Rev. Lett.* **2017**, *118*, 223603.

[25] J. N. Becker, J. Görlitz, C. Arend, M. Markham, C. Becher, *Nat. Commun.* **2016**, *7*, 13512.

**ADVANCED
SCIENCE NEWS**

www.advancedsciencenews.com

**ADVANCED
QUANTUM
TECHNOLOGIES**

www.advquantumtech.com

[26] M. Ruf, N. H. Wan, H. Choi, D. Englund, R. Hanson, *J. Appl. Phys.* **2021**, *130*, 070901.

[27] D. N. Jamieson, W. I. L. Lawrie, S. G. Robson, A. M. Jakob, B. C. Johnson, J. C. Mccallum, *Mater. Sci. Semicond. Process.* **2017**, *62*, 23.

[28] S. Pezzagna, D. Rogalla, D. Wildanger, J. Meijer, A. Zaitsev, *New J. Phys.* **2011**, *13*, 035024.

[29] Yu Zhou, Z. Mu, G. Adamo, S. Bauerdick, A. Rudzinski, I. Aharonovich, W-Bo Gao, *New J. Phys.* **2018**, *20*, 125004.

[30] T. Lühmann, R. John, R. Wunderlich, J. Meijer, S. Pezzagna, *Nat. Commun.* **2019**, *10*, 4956.

[31] J. L. Pacheco, M. Singh, D. L. Perry, J. R. Wendt, G. Ten Eyck, R. P. Manginell, T. Pluym, D. R. Luhman, M. P. Lilly, M. S. Carroll, E. Bielejec, *Rev. Sci. Instrum.* **2017**, *88*, 123301.

[32] K. C. Wong, S. L. Ng, K. O. Ho, Y. Shen, J. Wu, K. T. Lai, M. Y. Leung, W. K. Leung, D. B. R. Dasari, A. Denisenko, J. Wrachtrup, S. Yang, *Phys. Rev. Appl.* **2022**, *18*, 024044.

[33] X. J. Wang, H. H. Fang, F. W. Sun, H. B. Sun, *Laser Photonics Rev.* **2022**, *16*, 2100029.

[34] U. Wahl, J. G. Correia, R. Villarreal, E. Bourgeois, M. Gulka, M. Nesládek, A. Vantomme, L. M. C. Pereira, *Phys. Rev. Lett.* **2020**, *125*, 45301.

[35] T. Iwasaki, F. Ishibashi, Y. Miyamoto, Y. Doi, S. Kobayashi, T. Miyazaki, K. Tahara, K D. Jahnke, L J. Rogers, B. Naydenov, F. Jelezko, S. Yamasaki, S. Nagamachi, T. Inubushi, N. Mizuochi, M. Hatano, *Sci. Rep.* **2015**, *5*, 12882.

[36] E. Corte, S. Sachero, S. Ditalia Tchernij, T. Lühmann, S. Pezzagna, P. Traina, I. P. Degiovanni, E. Moreva, P. Olivero, J. Meijer, M. Genovese, J. Forneris, *Adv. Photonics Res.* **2022**, *3*, 2100148.

[37] M. E. Trusheim, N. H. Wan, K. C. Chen, C. J. Ciccarino, J. Flick, R. Sundararaman, G. Malladi, E. Bersin, M. Walsh, B. Lienhard, H. Bakhru, P. Narang, D. Englund, *Phys. Rev. B* **2019**, *99*, 075430.

[38] P. Wang, T. Taniguchi, Y. Miyamoto, M. Hatano, T. Iwasaki, *ACS Photonics* **2021**, *8*, 2947.

[39] Y. N. Palyanov, I. N. Kupriyanov, Y. M. Borzdov, *Carbon* **2019**, *143*, 769.

[40] P. Wang, T. Taniguchi, Y. Miyamoto, M. Hatano, T. Iwasaki, *ACS Photonics* **2021**, *8*, 2947.

[41] K. M. C. Fu, C. Santori, P. E. Barclay, R. G. Beausoleil, *Appl. Phys. Lett.* **2010**, *96*, 121907.

[42] A. M. Zaitsev, N. M. Kazuchits, K. S. Moe, J. E. Butler, O. V. Korolik, M. S. Rusetsky, V. N. Kazuchits, *Diamond Relat. Mater.* **2021**, *113*, 108255.

[43] S. Pezzagna, D. Rogalla, D. Wildanger, J. Meijer, A. Zaitsev, *New J. Phys.* **2011**, *13*, 035024.

[44] Y. F. Meng, C. Yan, H. Mao, R. J. Hemley, *Proc. Natl. Acad. Sci. USA* **2008**, *105*, 17620.

[45] E. Corte, G. Andrini, E. Nieto Hernández, V. Pugliese, Â. Costa, G. Magchiels, J. Moens, S. M. Tunhuma, R. Villarreal, L. M. C. Pereira, A. Vantomme, J. G. Correia, E. Bernardi, P. Traina, I. P. Degiovanni, E. Moreva, M. Genovese, S. Ditalia Tchernij, P. Olivero, U. Wahl, J. Forneris, *ACS Photonics* **2022**, *13*, 101.

[46] S. C. Kitson, P. Jonsson, J. G. Rarity, P. R. Tapster, *Phys. Rev. A* **1998**, *58*, 620.

[47] J. Görlitz, D. Herrmann, P. Fuchs, T. Iwasaki, T. Taniguchi, D. Rogalla, D. Hardeman, P. O. Colard, M. Markham, M. Hatano, C. Becher, *npj Quantum Inf.* **2022**, *8*, 45.

[48] I. A. Dobrinets, V. G. Vins, A. M Zaitsev, *HPHT-Treated Diamonds, Springer Series in Materials Science*, Vol. *181*, Springer, Berlin, Heidelberg **2013**.

[49] N. H. Wan, T. J. Lu, K. C. Chen, M. P. Walsh, M. E. Trusheim, L. De Santis, E. A. Bersin, I. B. Harris, S. L. Mouradian, I. R. Christen, E. S. Bielejec, D. Englund, *Nature* **2020**, *583*, 226.

[50] N. H. Wan, T. J. Lu, K. C. Chen, M. P. Walsh, M. E. Trusheim, L. De Santis, E. A. Bersin, I. B. Harris, S L. Mouradian, I. R. Christen, E S. Bielejec, D. Englund, *Sci Adv.* **2020**, *6*, 226.

[51] A. M. Berhane, K. Y. Jeong, C. Bradac, M. Walsh, D. Englund, M. Toth, I. Aharonovich, *Phys. Rev. B* **2018**, *97*, 165202.

[52] D. Chen, N. Zheludev, W. B. Gao, *Adv. Quantum Technol.* **2020**, *3*, 1900069.

[53] D. Chen, J. E. Fröch, S. Ru, H. Cai, N. Wang, G. Adamo, J. Scott, F. Li, N. Zheludev, I. Aharonovich, W. Gao, *Nano Lett.* **2022**, *22*, 6306.

[54] D. Chen, N. Zheludev, W. B Gao, *Appl. Phys. B* **2022**, *128*, 1900069.

[55] D. Chen, J. E. Fröch, S. Ru, H. Cai, N. Wang, G. Adamo, J. Scott, F. Li, N. Zheludev, I. Aharonovich, W. Gao, *Metrologia* **2019**, *56*, 6306.

2300010 (8 of 8)